Acta Cryst. (1997). B53, 176–180

Single-Crystal Neutron Diffraction Analysis of Anion–Cation Interactions in Perdeuteroacetylcholine Bromide at 100 K

NORMAN SHANKLAND,[a]* ALASTAIR J. FLORENCE[a] AND CHICK C. WILSON[b]

[a]*Department of Pharmaceutical Sciences, University of Strathclyde, Glasgow G1 1XW, Scotland, and* [b]*ISIS Facility, Rutherford Appleton Laboratory, Chilton, Didcot, Oxon OX11 0QX, England. E-mail: norman@pharmsci.strath.ac.uk*

(Received 20 May 1996; accepted 6 September 1996)

Abstract

The interaction of the neurotransmitter acetylcholine with receptor binding sites has been well studied over the years, but much is still unknown about how intermolecular forces govern the lock-and-key fit. Here we present an analysis of cation–anion hydrogen-bond interactions in a single crystal of perdeuteroacetylcholine bromide, using pulsed neutron diffraction data to refine the X-ray crystal structure. The molecule crystallizes in space group $P2_1/n$, with $a = 10.951(4)$, $b = 13.396(8)$, $c = 7.072(4)$ Å, $\beta = 108.88(3)^\circ$, $Z = 4$. The final refinement included anisotropic temperature factors on all atoms and converged to $wR(F) = 0.055$ (244 parameters). The pyramidal configuration of C—D···Br^- contacts observed in the crystal is in good agreement with *ab initio* molecular orbital predictions of favoured configuration and is consistent with a modest polarization of C—D bonds close to the N atom. There is evidence that close contact with Br^- is hindered by the repulsive influence of the ester O atoms, dependent on the conformation of the acetylcholine cation. This is the most detailed picture to date of close interatomic contacts around the cation and analogies are drawn with the bonding of acetylcholine to its receptors.

1. Introduction

The way in which an acetylcholine (ACh) cation binds to a receptor requires a knowledge of the three-dimensional molecular structures of the receptor and cation, and an understanding of the non-covalent interatomic forces bonding the cation to the receptor. There are no high-resolution structures available for muscarinic or nicotinic ACh receptors [*cf.* the ACh esterase enzyme (Sussman *et al.*, 1991, Harel *et al.*, 1993)], although progress in the last few years has seen the nicotinic structure determined by electron microscopy, in the open- and closed-channel states, at 9 Å resolution (Unwin, 1993, 1995). There is a growing body of evidence pointing to the importance of electrostatic attraction between the cation and the quadrupole moment of aromatic amino acid fragments at receptor binding sites, the so-called cation–π interaction (Dougherty, 1996). Although this evidence is recent, the idea that the ACh cation may show orientational preferences with respect to regions of receptor negative electrostatic potential was put forward over a decade ago (Rosenfield & Murray-Rust, 1982). Our study of perdeuterated ACh molecular structure includes accurate determination of D-atom positions and examines anion interactions with the D atoms that surround the quaternary ammonium group.

In the first instance, we have exploited the power of low-temperature neutron diffraction to accurately determine all atomic positions in a single crystal of fully deuterated ACh bromide ($C_7D_{16}O_2N^+Br^-$). Deuteration improves the accuracy of the neutron experiment in two ways. First, it reduces the incoherent background scattering observed with protonated samples and, second, deuterium has a coherent scattering length of significantly larger magnitude than hydrogen. This means that while neutrons will detect H-atom positions with good accuracy and precision, the situation is still better for deuterium, assuming that any isotope effects on the molecular structure are negligible in the context of the experiment.

2. Experimental

Deuterated ACh bromide was supplied by MSD Isotopes. Large colourless, hygroscopic single crystals were obtained by slow evaporation from saturated ethanol solution and stored in airtight containers under nitrogen prior to the diffraction experiment.

Diffraction data were collected from a single crystal on SXD at the ISIS spallation neutron source (Wilson, 1990, 1996) using the time-of-flight Laue diffraction method. The crystal and data collection parameters are summarized in Table 1. The crystal was mounted on a two-circle orienter (χ, φ) in a

Table 1. *Data collection and refinement parameters for perdeuteroacetylcholine bromide*

Instrumental	
Diffractometer	SXD neutron time-of-flight Laue diffractometer at ISIS
Temperature (K)	100
Detector	64 × 64 3 mm pixel scintillator, placed 128 mm from sample
Angular range (°)	$2\theta = 110 \pm 35$
Wavelength range (Å)	0.48–4.8
Sample	
Compound	Acetylcholine bromide (99.3 atom% D)
Formula	$C_7D_{16}O_2N^+.Br^-$
Molecular weight	242.22
Recrystallizing solvent	Ethanol
Crystal size (mm)	5 × 3 × 1.5
Refinement	
Space group	$P2_1/n$
Unit-cell refinement	172 reflections
Unit cell (Å, °)	$a = 10.951(4)$, $b = 13.396(8)$, $c = 7.072(4)$; $\beta = 108.88(3)$
Volume (Å^3)	981.6(9)
Calculated density (g cm^{-3})	1.639
Data frames	25, allowing for much overlap between adjacent frames and hence measurement of many equivalent reflections
Maximum $\sin\theta/\lambda$ (Å^{-1})	1.22
Measured reflections	7094
Unique reflections	3101 ($I > 3\sigma I$)
Index limits	$0 < h < 25$, $0 < k < 33$, $-17 < l < 14$
Refined parameters	244
Thermal parameters	All atoms anisotropic
Agreement factors	$R(F) = 0.072$
	$wR(F) = 0.055$
	$w = [2F_o/\sigma(F_o^2)]^2$

Displex closed-cycle refrigerator (CCR) helium cryostat. The data collection temperature was computer controlled to ±1 K and was measured by a Rh–Fe thermocouple situated ~10 mm from the sample at the CCR head. Collection of a complete structure factor set in this diffraction geometry consists of the accumulation of a series of data frames, each containing a large volume of reciprocal space and collected with a stationary crystal and detector arrangement. Typical frame exposure times in this experiment were around 45 min, yielding several hundred observed reflections in each frame. This data collection method, with a large degree of overlap maintained between adjacent frames, leads to a large overdetermination of equivalent reflections in the data sets. It is clear from subsequent normalization and merging procedures that there was no measurable change in the scattering power of the crystal during the data collection. The overlap between frames also to some extent mitigates the problem that different $\sin\theta/\lambda$ ranges are accessed in different parts of the detector.

With many reflections determined within each frame, determination and refinement of the UB matrix is straightforward. Each three-dimensional data histogram was searched for peaks and these were indexed using the UB matrix. The final unit-cell dimensions were determined using reflections taken from a wide range of data frames, while for peak integration a local UB matrix for each frame was used. The peaks were integrated using a profile fitting approach based on the known analytical shape of the reflections in the time-of-flight direction, well understood from the characteristics of the ISIS source and moderator. The function used, a Gaussian convoluted with a decaying exponential function, reproduces the peak shape well. The variable parameters in this fit are the Gaussian height and width and the time constant of the exponential, all of which vary with time-of-flight. This method is sensitive and reliable in the integration of both strong and weak peaks. Reflections for which this profile fitting procedure failed after four attempts on different integration windows were excluded from the data set, thus resulting in a somewhat reduced occurrence of very weak or 'unobserved' peaks in the final data set. This recently implemented intensity extraction procedure is currently under further development to improve the handling of these weak or unobserved reflections. It should also be noted that the method of data collection occasionally allows for the observation of very high $\sin\theta/\lambda$ reflections, even when no real attempt has been made to measure in this region. For these reasons, the $\sin\theta/\lambda$ limit of the data is difficult to estimate precisely, but the planned improvements to the weak peak handling will help mitigate this problem in the future.

The reflection intensities were normalized to the wavelength-dependent incident beam profile using the incoherent scattering from a polycrystalline vanadium sample. Semi-empirical absorption corrections were also applied at this stage, using the vanadium and perdeuterated ACh bromide sample scattering. The resulting intensities were reduced to structure factors, giving a data set as detailed in Table 1. The data were used in the Cambridge Crystallographic Subroutine Library (Brown & Matthewman, 1993) least-squares refinement program *SFLSQ*, to apply a variable wavelength extinction correction based on the Becker–Coppens formalism (Becker & Coppens, 1974*a*,*b*) using a Gaussian model with one variable parameter, the mosaic spread. The resulting corrected structure factors were merged (see Table 1) and refined as described below.

3. Structure refinement

The corrected and merged data were used to refine the atomic coordinates and thermal parameters by full least-squares methods on F within the program *GSAS* (Larsen & Von Dreele, 1994), using the X-ray structure (Svinning & Sørum, 1975) as a starting model. Subsequently, it was found that the cell metric (Table 1), and that of the original study, is also consistent with a C-centred orthorhombic cell of twice the volume of

Table 2. *Fractional atomic coordinates and equivalent isotropic displacement parameters ($Å^2$) at 100 K*

$$U_{eq} = (1/3)\sum_i \sum_j U^{ij} a_i^* a_j^* \mathbf{a}_i . \mathbf{a}_j .$$

	x	y	z	U_{eq}
Br1	0.28565 (14)	−0.38391 (13)	−0.35897 (19)	0.0126
C1	0.42119 (16)	0.34295 (14)	−0.45830 (19)	0.0119
C2	0.41995 (16)	0.34731 (14)	−0.1140 (2)	0.0115
C3	0.58255 (16)	0.43982 (13)	−0.2072 (2)	0.0112
C4	0.59914 (15)	0.26032 (13)	−0.18782 (19)	0.0090
C5	0.54206 (16)	0.15707 (13)	−0.22955 (19)	0.0104
C6	0.60772 (15)	0.10747 (13)	−0.50270 (18)	0.0101
C7	0.56690 (18)	0.09716 (15)	−0.7250 (2)	0.0155
N1	0.50468 (10)	0.34599 (9)	−0.24352 (12)	0.0083
O1	0.50884 (17)	0.13197 (15)	−0.4387 (2)	0.0115
O2	0.71792 (17)	0.10008 (17)	−0.3910 (2)	0.0145
D11	0.3652 (2)	0.27621 (17)	−0.4842 (3)	0.0229
D12	0.4857 (2)	0.34201 (18)	−0.5506 (2)	0.0253
D13	0.3628 (2)	0.40876 (18)	−0.4872 (3)	0.0254
D21	0.3595 (2)	0.28126 (18)	−0.1395 (3)	0.0262
D22	0.4818 (2)	0.35192 (19)	0.0414 (3)	0.0266
D23	0.3600 (2)	0.41409 (19)	0.1531 (3)	0.0280
D31	0.6430 (2)	0.43939 (18)	−0.3046 (3)	0.0253
D32	0.6421 (2)	0.44197 (17)	−0.0514 (3)	0.0246
D33	0.5163 (2)	0.50213 (16)	−0.2430 (3)	0.0247
D41	0.6688 (2)	0.27269 (16)	−0.2669 (2)	0.0191
D42	0.6484 (2)	0.26956 (15)	−0.0274 (2)	0.0193
D52	0.4514 (2)	0.14829 (18)	−0.1946 (3)	0.0237
D51	0.6115 (2)	0.10337 (17)	−0.1428 (2)	0.0228
D71	0.4644 (2)	0.0833 (2)	−0.7895 (3)	0.0348
D72	0.6234 (2)	0.0399 (2)	−0.7670 (3)	0.0323
D73	0.5884 (3)	0.1669 (2)	−0.7830 (3)	0.0431

the monoclinic cell. This would imply the existence of reflections of the type $([h-k]/2, 1, -h)$ if the orthorhombic cell was the correct choice. Extensive searches through our data revealed no reflections inconsistent with the monoclinic cell choice to support the adoption of the C-centred orthorhombic cell. All refinements and further calculations were thus carried out in the monoclinic space group as in the X-ray study. The final refinement included anisotropic temperature factors on all atoms and converged to $wR(F) = 0.055$ (24 parameters), $w = [2F_o/\sigma(F_o^2)]^2$.

4. Results and discussion

The refined molecule is shown in Fig. 1, with atomic coordinates and thermal parameters given in Table 2, and bond lengths and angles in Table 3.* For C, N and O atoms the difference between the nuclear positions observed with neutrons, and the electron density maxima observed with X-rays, is insignificant. The single-crystal neutron refinement therefore gives C—C, C—N and C—O bond lengths which are in good agreement with the X-ray results. The mean C—D bond length, however, is a significant improvement upon the mean C—H value obtained with X-rays, with e.s.d.'s smaller by a factor of 10. The N1—C4—C5—O1 and C4—C5—O1—C6 torsion angles which define the overall *gauche-gauche* conformation of the cation in the crystal are

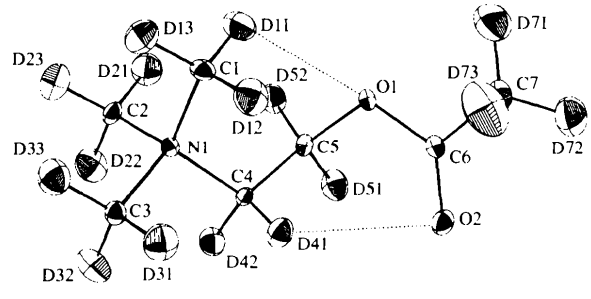

Fig. 1. *ORTEP*II (Johnson, 1971) plot of the ACh cation, with anisotropic thermal ellipsoids plotted at 50% probability. The dashed lines indicate the intramolecular interactions C1—D11···O1 = 2.446 (3) and C4—D41···O2 = 2.591 (3) Å.

Table 3. *Perdeuteroacetylcholine bromide. Covalent bond lengths (Å) and angles (°) for the neutron refinement (e.s.d.'s in parentheses), with X-ray values (Svinning and Sørum, 1975) for comparison*

	Neutron	X-ray		Neutron	X-ray
N1—C1	1.499 (1)	1.496 (5)	C1—D11	1.066 (3)	0.90 (3)
N1—C2	1.500 (2)	1.498 (6)	C1—D12	1.106 (3)	0.93 (4)
N1—C3	1.494 (2)	1.502 (4)	C1—D13	1.069 (3)	0.98 (4)
N1—C4	1.510 (2)	1.513 (4)	C2—D21	1.085 (3)	0.92 (4)
C4—C5	1.507 (2)	1.500 (5)	C2—D22	1.090 (2)	1.00 (5)
C5—O1	1.444 (2)	1.452 (5)	C2—D23	1.091 (3)	0.97 (4)
C6—O1	1.342 (3)	1.358 (5)	C3—D31	1.099 (3)	0.91 (4)
C6—O2	1.214 (2)	1.192 (4)	C3—D32	1.084 (2)	0.94 (3)
C6—C7	1.495 (2)	1.487 (6)	C3—D33	1.081 (3)	1.01 (3)
			C4—D41	1.094 (3)	0.93 (4)
			C4—D42	1.094 (2)	0.94 (3)
			C5—D51	1.082 (2)	1.03 (3)
			C5—D52	1.104 (3)	0.96 (4)
			C7—D71	1.082 (3)	0.95 (5)
			C7—D72	1.085 (3)	1.00 (5)
			C7—D73	1.077 (4)	1.00 (5)
			Average C—D	1.087	0.96

	Neutron	X-ray		Neutron	X-ray
C1—N1—C2	108.9 (1)	109.8 (3)	D11—C1—D12	109.3 (2)	–
C1—N1—C3	108.9 (1)	108.6 (3)	D11—C1—D13	112.6 (2)	–
C1—N1—C4	112.7 (1)	112.2 (3)	D11—C1—N	108.99 (16)	–
C2—N1—C3	108.5 (1)	108.3 (3)	D12—C1—D13	110.7 (2)	–
C2—N1—C4	110.9 (1)	110.7 (3)	D12—C1—N	107.56 (15)	–
C3—N1—C4	106.9 (1)	107.1 (2)	D13—C1—N	107.61 (16)	–
N1—C4—C5	116.2 (1)	116.4 (3)	D21—C2—D22	111.1 (2)	–
C4—C5—O1	111.4 (1)	111.6 (3)	D21—C2—D23	110.0 (2)	–
C5—O1—C6	116.0 (1)	115.7 (3)	D21—C2—N1	110.73 (18)	–
O1—C6—C7	112.2 (1)	111.3 (3)	D22—C2—D23	109.6 (2)	–
O1—C6—O2	122.8 (2)	122.8 (4)	D22—C2—N1	108.10 (19)	–
C7—C6—O2	124.9 (2)	125.9 (4)	D23—C2—N1	107.18 (18)	–
D31—C3—N1	108.28 (17)	–	D31—C3—D32	110.5 (2)	–
D31—C3—D33	110.6 (2)	–	D32—C3—D33	110.8 (2)	–
D32—C3—N1	108.64 (17)	–	D33—C3—N1	107.86 (16)	–
D41—C4—N1	106.47 (16)	–	D41—C4—C5	110.64 (18)	–
D41—C4—D42	108.73 (19)	–	D42—C4—N1	104.54 (15)	–
D42—C4—C5	109.93 (16)	–	D51—C5—C4	109.18 (15)	–
D51—C5—O1	108.92 (18)	–	D51—C5—D52	108.6 (2)	–
D52—C5—C4	113.58 (19)	–	D52—C5—O1	104.94 (15)	–
D71—C7—D72	111.6 (2)	–	D71—C7—D73	108.3 (3)	–
D71—C7—C6	112.1 (2)	–	D72—C7—D73	107.2 (3)	–
D72—C7—C6	110.48 (16)	–	D73—C7—C6	107.03 (19)	–

* Lists of anisotropic displacement parameters and structure factors have been deposited with the IUCr (Reference: AN0532). Copies may be obtained through The Managing Editor, International Union of Crystallography, 5 Abbey Square, Chester CH1 2HU, England.

77.87(18) and 76.3(2)°, respectively, in good agreement with the X-ray values.

The C—D···O interactions identified in Fig. 1 are favoured by the delocalization of positive charge from the nitrogen (see below), which results in a decrease in electron density around D11 and D41. The observed distances are consistent with the results of a neutron diffraction analysis of C—H···O interactions in crystalline amino acids (Jeffrey & Maluszynska, 1982), where C—H···O distances ranged from 2.16 to 2.65 Å (mean = 2.45 Å). Although these contacts are significant, it seems unlikely that they contribute much to the conformational stability of the ACh cation. The significance really lies in the fact that *all* of the D atoms surrounding the nitrogen seek close contact with an electronegative atom, either O or Br^-.

The deuteriums on C1 to C5 of the ACh cation make a total of 11 short (2.7–3.2 Å), and one long (4.0 Å), contacts to four symmetry-related bromide ions (Fig. 2, Table 4). Each anion is positioned over a

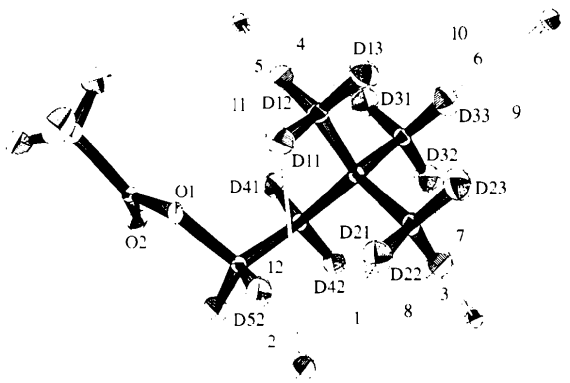

Fig. 2. An alternative view of the ACh cation, showing four symmetry-related bromide ions clustering around the quaternary ammonium group. Each bromide ion lies close to the centroid of a plane formed by three deuteriums. The covalent bonds are thicker than those depicted in Fig. 1 in order to distinguish the cation from the non-covalent bromide ion contacts, which are indicated by the hollow bonds numbered 1 to 12.

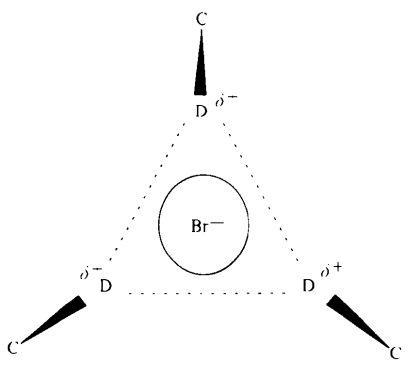

Fig. 3. A schematic representation of a bromide ion positioned over a triangular plane of D atoms.

Table 4. *Distances (Å) for the numbered D···Br⁻ contacts shown in Fig. 2*

Contact 12 is significantly longer ($>3\sigma$) than the mean of distances 1–11 (2.92 ± 0.16 Å).

	D atom	Symmetry-related bromide ion	Distance	Contact
Plane 1	D33	$x, 1+y, z$	2.836 (3)	6
	D23		3.056 (3)	9
	D13		3.122 (3)	10
Plane 2	D22	$1-x, -y, -z$	2.830 (2)	3
	D32		2.858 (2)	7
	D42		3.009 (2)	8
Plane 3	D31	$1-x, -y, -1-z$	2.834 (3)	4
	D12		2.836 (3)	5
	D41		3.214 (3)	11
Plane 4	D21	$\frac{1}{2}-x, \frac{1}{2}+y, -\frac{1}{2}-z$	2.722 (3)	1
	D52		2.776 (3)	2
	D11		3.977 (3)	12

Table 5. *Distances (Å) and angles ( ) between D atoms in planes 1–4*

x is the distance (Å) between the centroid of the triangle and the point where a perpendicular from Br^- intersects the plane.

	x				
Plane 1	0.393	D13···D33	2.343	D13···D33···D23	61.1
		D33···D23	2.330	D33···D23···D13	59.8
		D23···D13	2.374	D23···D13···D33	59.2
Plane 2	0.351	D22···D42	2.314	D22···D42···D32	62.2
		D42···D32	2.316	D42···D32···D22	58.9
		D32···D22	2.390	D32···D22···D42	59.0
Plane 3	0.633	D12···D41	2.511	D12···D41···D31	60.2
		D41···D31	2.256	D41···D31···D12	65.2
		D31···D12	2.399	D31···D12···D41	54.6
Plane 4	0.746	D11···D52	2.602	D11···D52···D21	61.6
		D52···D21	2.144	D52···D21···D11	68.4
		D21···D11	2.468	D21···D11···D52	50.0

plane of three deuteriums, in a pyramidal configuration. This is shown schematically in Fig. 3, with the distances and angles between the deuteriums in each of the four planes given in Table 5. *Ab initio* molecular orbital calculations on the isolated tetramethylammonium and ACh cations (Barrett, Roberts, Burgen & Clore, 1983) show that the positive charge formally located on the nitrogen is delocalized extensively onto the methyl groups, with a decrease in electron density around the H atoms. The calculations also suggest that the pyramidal geometry is favoured over the other possible configurations for an interacting halide ion. This is generally consistent with what we observe in the crystal structure, except at plane 4, where the pyramidal geometry is distorted by a long D11···Br^- distance (contact 12 in Fig. 2). It is important to note that, in general, small spherical anions will readily occupy sites of favourable electrostatic interaction in a crystal lattice, because they are relatively free from steric constraints (Rosenfield & Murray-Rust, 1982; Jeffrey & Saenger, 1991). This enables us to make a valid comparison between what we observe in the crystal structure and *ab initio* predictions of favoured configuration.

The most striking feature in the analysis of D···Br^- distances is the distortion of the pyramidal geometry at plane 4. It is clear that this is a consequence of the conformation of the ACh cation, which places O1 in close proximity to D11. Thus, O1···Br^- repulsion hinders the anion from adopting a preferred position close to the centroid of plane 4, particularly as O1 carries a significant partial negative charge (Fig. 4). A smaller distortion of the geometry at plane 3 occurs due to the proximity of O2 to D41 (Fig. 1).

There is an obvious analogy with cation–receptor interactions, where O1 and O2 might well influence the availability of specific cation H atoms to interact with regions of negative electrostatic potential on the receptor. 96% of non-covalent interatomic contacts in this crystal structure (out to a distance of ~3.5 Å) involve deuterium, underlining the importance of deuterium in determining how the molecules pack in the crystal. By analogy, contacts to H atoms will play a key role in the bonding of ACh to its receptors. Observations in this study are certainly consistent with a modest polarization of C—D bonds close to the nitrogen. More importantly, the role of O1 and O2 in receptor binding may well extend beyond the possibility of intermolecular hydrogen bonding. The cation is flexible enough to adopt conformations which bring oxygen into close contact with H atoms in planes 2, 3 and 4, but not plane 1. It is therefore interesting to speculate that unhindered interaction with plane 1 has evolved as a common feature of binding to all ACh receptor types, while the specific contacts with planes 2, 3 and 4 vary with cation conformation at the different receptors. Although we have reached our conclusions based on the study of a single fixed conformation of the ACh cation, the general idea of electronegative atoms competing to interact with cation hydrogens will apply, irrespective of the conformation of the cation bound to a receptor.

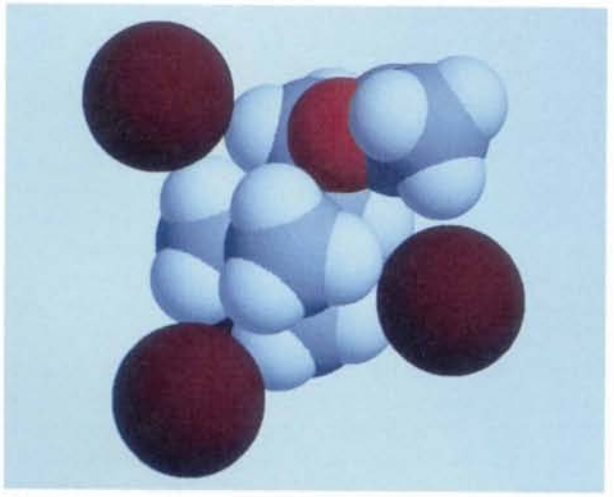

Fig. 4. A space-filling model of the ACh cation using van der Waals radii, showing bromide ions positioned over three of the four deuterium planes [plane 4 top, plane 1 bottom and plane 3 to the right (plane 2 obscured in this view)]. The model clearly shows why bromide cannot adopt a central position over plane 4 – to do so would bring the anion prohibitively close to the O atom.

5. Conclusions

(1) The single-crystal neutron refinement at 100 K provides accurate atomic positions and thermal parameters for all atoms in perdeuterated ACh bromide.

(2) The pyramidal configuration of C—D···Br^- interactions observed in the single crystal is consistent with *ab initio* molecular orbital predictions of the optimal configuration for an anion interacting with an isolated cation.

(3) The conformation of the cation places O1 in close contact with the D11 atom, hindering the D11···Br^- interaction and distorting the pyramidal configuration at plane 4.

We wish to thank Dr Kenneth Shankland at ISIS and Dr John Connolly at University of Strathclyde for valuable discussions. Access to ISIS is made possible through EPSRC and BBSRC.

References

Barrett, A. N., Roberts, G. C. K., Burgen, A. S. V. & Clore, G. M. (1983). *Mol. Pharmacol.* **24**, 443–448.
Becker, P. & Coppens, P. (1974*a*). *Acta Cryst.* A**30**, 129–147.
Becker, P. & Coppens, P. (1974*b*). *Acta Cryst.* A**30**, 148–153.
Brown, P. J. & Matthewman, J. C. (1993). Rutherford Appleton Laboratory Report, RAL-93-009.
Dougherty, D. A. (1996). *Science*, **271**, 163–168.
Harel, M., Schalk, I., Ehret-Sabattier, L., Bouet, F., Goeldner, M., Hirth, C., Axelsen, P., Silman, I. & Sussman, J. L. (1993). *Proc. Natl Acad. Sci. USA*, **90**, 9031–9035.
Jeffrey, G. A. & Maluszynska, H. (1982). *Int. J. Biol. Macromol.* **4**, 173–185.
Jeffrey, G. A. & Saenger, W. (1991). *Hydrogen Bonding in Biological Structures*, Ch. 11. Berlin: Springer-Verlag.
Johnson, C. K. (1971). *ORTEP*II. Report 3794, revised. Oak Ridge National Laboratory, Tennessee, USA.
Larsen, A. C. & Von Dreele, R. B. (1994). Report LAUR 86-748. Los Alamos National Laboratory, Los Alamos, USA.
Rosenfield Jr, R. E. & Murray-Rust, P. (1982). *J. Am. Chem. Soc.* **104**, 5427–5430.
Sussman, J. L., Harel, M., Frolow, F., Oefner, C., Goldman, A., Toker, L. & Silman, I. (1991). *Science*, **253**, 872–878.
Svinning, T. & Sørum, H. (1975). *Acta Cryst.* B**31**, 1581–1586.
Unwin, N. (1993). *J. Mol. Biol.* **229**, 1101–1124.
Unwin, N. (1995). *Nature*, **373**, 37–43.
Wilson, C. C. (1990). *Neutron Scattering Data Analysis*, edited by M. W. Johnson, Ch. 2. Bristol: Adam Hilger.
Wilson, C. C. (1996). *J. Mol. Struct.* In the press.